ISSN: 0067-2904

The Influence of CeO_2 Concentration on Some Physical Properties of Y_2O_3 Thin Films

Ikram Kamel abd Karem*, Suhad A. Hamdan
Department of Physic, College of science, University of Baghdad, Baghdad, Iraq

Received: 7/4/2021 Accepted: 24/8/2021 Published: 30/6/2022

Abstract

Thin films of pure yttrium oxide (Y_2O_3) and doped with cerium oxide (CeO_2) were prepared by the chemical spray pyrolysis(CSP)method. The structural, optical and electrical properties of the prepared films were investigated. The analysis of X-ray diffraction (XRD) thin films revealed that the undoped and doped Y_2O_3 were amorphous with a broad hump around 27^o and narrow humps around 48^o and 62^o for all samples. Except for the Y_2O_3:6wt.%CeO_2 thin film, all had signal preferential orientation along the (100) plane at $2\theta=12.71^o$ which belongs to CeO_2, Field emission scanning electron microscopic (FE-SEM) images confirmed the formation of the nanosized particles which resembles circles and others revealed rods and balls shape. UV-Vis spectra study showed peak absorption at a wavelength of 305 nm, with blue shift due to quantum confinement, and this also happened for the doped films, with direct energy band gaps. The photoluminescence spectra (PL) of undoped Y_2O_3 and doped thin films showed an emission peak at 365 nm at the same wavelength of all the prepared samples with a slight difference. All prepared films show three activation energies except Y_2O_3:6wt.%CeO_2 film has two activation energies. From I-V characteristic curves, the prepared films have Schottky behavior except Y_2O_3:6wt.%CeO_2 film, which displayed ohmic behavior. Y_2O_3:6wt.%CeO_2 fabricated device revealed good photosensitivity for VIS and IR wavelength.

Keywords: Yttrium Oxide, optical properties, surface morphology, photodetector, cerium oxide.

تاثير تركيز اوكسيد السيريوم على بعض الخصائص الفيزياوية لاغشية اوكسيد اليتريوم الرقيقة

اكرام كامل عبد كريم* ، سهاد عبد الكريم حمدان
قسم الفيزياء، كلية العلوم، جامعة بغداد، بغداد، العراق

الخلاصة

تم تحضير أغشية رقيقة من أكسيد الإيتريوم النقي Y_2O_3 والمشوب بأكسيد السيريوم CeO_2 بطريقة الرش الكيميائي الحراري. تم فحص الخواص البصرية والهيكلية والكهربائية للأغشية المحضرة. كشف تحليل حيود الأشعة السينية (XRD) للأغشية الرقيقة أن الطبيعة العشوائية Y_2O_3 مع سنام عريض حول الزاوية 27 درجة وسنام ضيقة حول الزاويا 48 درجة و 62 درجة لجميع العينات. باستثناء Y_2O_3 المشوب ب 6% سيريوم اوكسيد ، كان له اتجاه تفضيلي على طول المستوى (100) عند الزاوية 12.74 يعود إلى CeO_2.أكدت الصور المجهرية لمسح الانبعاث الإلكترونى (FE-SEM) تكوين حسيمات ذات حجم نانوي

*Email: ikram.kareem1204@sc.uobaghdad.edu.iq

تشبه الدوائر وأخرى تكشف عن قضبان وكرات معًا. تم إجراء دراسة طيف الأشعة فوق البنفسجية والمرئية (UV–VIS) التي أظهرت ذروة الامتصاص عند الطول الموجي 305 نانومتر ، مع ازاحة زرقاء بسبب الحصر الكمي ، وقد حدث هذا أيضًا للاغشية المشوبة ، مع وجود فجوات مباشرة في نطاق الطاقة. أطياف PL لجسيمات Y_2O_3 النانوية الغير مشوبة والمشوبة تظهر ذروة الانبعاث (عند 365 نانومتر) بنفس الطول الموجي لجميع العينات المحضرة مع اختلاف طفيف. تُظهر جميع الاغشية المحضرة ثلاث طاقات تنشيط ما عدا الغشاء Y_2O_3 المشوب بنسبة 6% CeO_2 يحتوي على طاقتي تنشيط. خصائص I–V للاغشية تسلك سلوك شوتكي باستثناء غشاء Y_2O_3 المشوب بنسبة 6% CeO_2 سلوك أومي. اظهر الجهاز المصنع من الغشاء Y_2O_3 المشوب بنسبة 6% CeO_2 حساسية ضوئية جيدة للاطوال الموجية المرئية والأشعة تحت الحمراء.

1. Introduction

Yttrium oxide (Y_2O_3), an important member of rare earth compounds, has been actively studied in recent years. It possesses excellent physical and chemical properties such as a high melting point of 2698^{o}K, high corrosion resistance and optical transparency over a wide wavelength range. Due to its good physical and chemical properties, Y_2O_3 has been widely used in various areas, such as luminescence, advanced ceramics, catalysts, and insulators [1]. This material could be synthesized via several methods, including gas-phase condensation [2], sol-gel [3], pyrolysis [4], solvothermal [5], and hydrothermal techniques [6].

In this work, undoped and doped Y_2O_3 films were fabricated using the chemical spray pyrolysis (CSP) deposition method. The structural, morphological, optical and electrical properties of the prepared samples were studied.

2. Experimental Methods

2.1. Sample preparation

Yttrium nitrate hexahydrate and cerium nitrate hydrate [$Y(NO_3)_3{\cdot}6H_2O$ and $Ce(NO_3)_4{\cdot}H_2O$] with (0.1M) were dissolved separately in distilled water and ethanol at a ratio of 80:20. Then stirred separately on a magnetic stirrer for (15-20) min to completely dissolve the salts. By this way, the precursors were prepared which were the source of yttrium and cerium ions. The yttrium precursors were doped with (2, 4, 6, 8, and 10) wt.% CeO_2 and stirred for 10 min. After that, the solution pH was measured; its value was between (4-5). Thin films were deposited on glass and Si wafer substrates using chemical spray pyrolysis method at 373 ^{o}K temperature of the substrate and at 30 min deposition time. The distance from the nozzle to the plate was 20 cm.

2.2. Measurement procedures

The structure of undoped and doped with (2, 4, 6, 8, and 10) %wt CeO_2 thin films of Y_2O_3 was examined with an X-ray diffractometer (XRD-6000 Labx, supplied by Shimadzu, X-ray source is Cu). The target was CuKα at a wavelength of 1.5406Å. Film morphology was analyzed with field emission scanning electron microscope (MIRA3 model – TE-SCAN). UV-Visible spectrophotometer (190-1100 nm) (Meterrech SP – 8001)was used to study the optical properties of the prepared thin films, such as optical energy gap, absorbance, and transmittance, based on transmission and absorbance spectra. The output data of wavelength transmittance were used in a computer program to deduce the optical energy bandgap.

The photoluminescence spectra of the prepared films at room temperature were measured using RF-551 spectrofluorometric detector, 200 W Hg (Xe) lamp, from (200-900) nm, using excitation wavelength which is the maxima of optical absorption spectra. Van der Pauw (Ecopia HMS-3000) was used for the Hall measurements with a 0.55 Tesla magnetic field. The conductivity as a function of temperature was used to measure the activation energy for the prepared films on glass substrates. The prepared films were heated in an oven starting at 298ºK up to 473 ºK with a step of 283ºK. The temperature was recorded by (MANFREDI L7). (FARNELL E350) A power supply was used to supply the bias voltage. The current was

measured with a multimeter ("USA origin, Keithley-616 Digital Electrometer"). Electrical resistance can be measured directly for all steps with a digital electrometer. Keithley-2450 was used for the IV measurements. The fabricated Y_2O_3 films were with a thickness of 515.6 nm. The film thickness measurements were performed with the use reflectance in Iraqi Ministry of science and technology optical metrology system using Stellar Nat Inc.

3. Results and Discussion

3.1. Structural properties

1. XRD

XRD patterns of the undoped and doped thin films are compared in Figure 1. The XRD patterns showed the amorphous nature of the thin films with a broad hump around 27° and narrow humps around 48° and 62° for all samples. This result is in agreement with previous reported results[7,8]. Y_2O_3:6wt.%CeO_2 thin film had a signal preferential orientation along the (100) plane at 2θ of 12.71° belonging to CeO_2 in agreement with standard JCPDS card (card No. 00-044-1001) of CeO_2.

Crystallite size (D) was estimated from Scherrer equation [9]:

$$D = \frac{K.\lambda}{\beta.\cos\theta} \quad (1)$$

Where: β is the full width at half-maximum (FWHM), θ is the angle of the diffraction peak, K is the shape factor (0.94), and λ is 0.15405 nm which is the wavelength of the X-ray source . The calculated crystallite size (D) was 20.3193 nm.

d_{hkl} is the interplaner spacing which was calculated using Bragg law [9]:

$$n\lambda = 2d_{hkl}\sin\theta \quad (2)$$

$(d_{hkl})exp.$ is found to be 6.943A° while interplaner spacing standard $(d_{hkl})std.$ is 7.24 A° (JCPDS card, card No. 00-044-1001 of CeO_2).

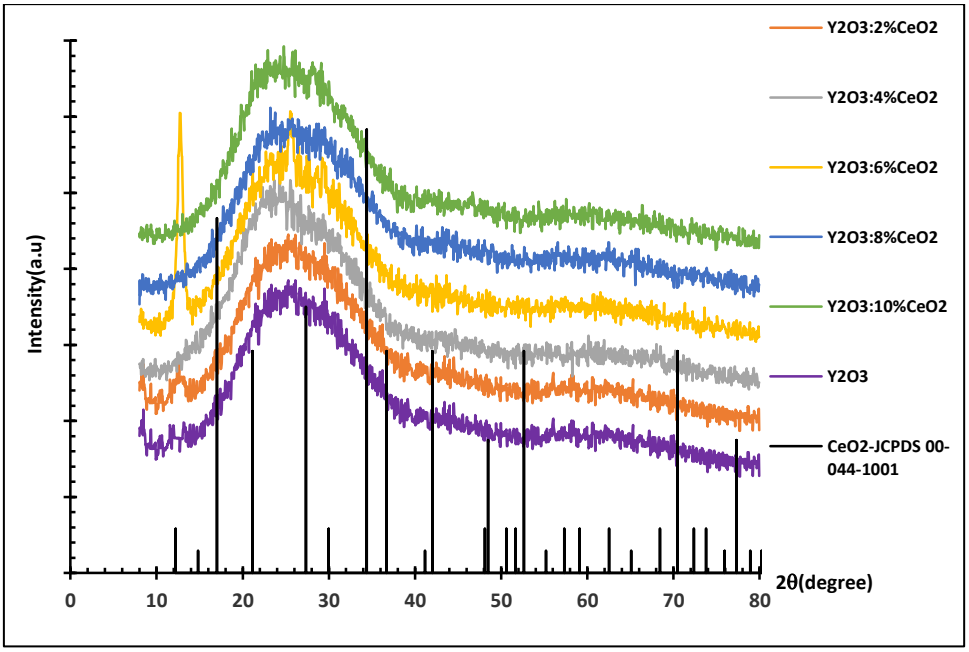

Figure 1- XRD patterns for undoped and doped with (2, 4, 6, 8, and 10)%wt. ceria of yttria thin films.

2. FE-SEM

Figure 2 illustrates the FE-SEM images, with different magnifications, of undoped and doped with (2 and 10) wt.% CeO_2, Y_2O_3 thin films. The image of the undoped Y_2O_3 sample (Figure 2a) revealed the nanorod-shaped particles and average particle size in the range of about 112.1075 nm. Doping with 2 and 10 wt% CeO_2 influenced the morphology of the

ground of the sample, as shown in Figures 2b and 2c, respectively. Figure 2b revealed that the particles are of circular shape with smooth surface, while Figure 2c shows the particles as balls shaped and average particle size in the range of about 69.87 nm.

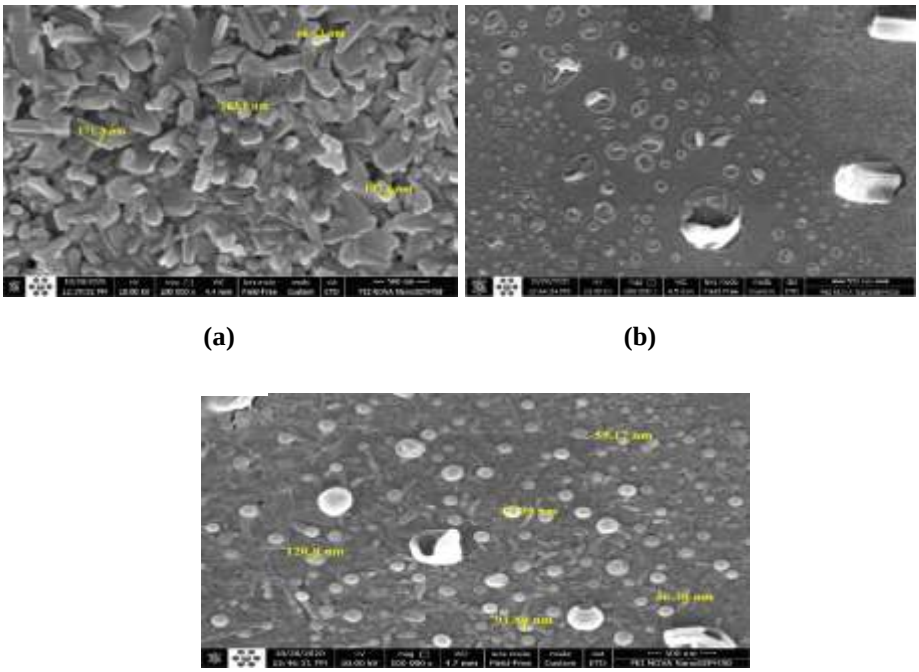

(a) **(b)**

(c)

Figure 2-FESEM images of (a) undoped Y_2O_3 thin film,(b)doped with 2% CeO_2 , and (c) doped with 10% CeO_2

3. Optical properties

1. UV-Vis Spectral study

The optical absorbance spectra of undoped and doped with CeO_2, Y_2O_3 thin films are shown in Figure 3. The spectra show a strong blue shift at 305 nm, which is in agreement with other researchers [7, 8]. There was a blue shift in absorbance edges toward low wavelengths for the doped thin films, which may be related to the decrease of the particles size and is attributed to the quantum confinement [10]. Nonsystematic increase of absorbance with doping in the UV range may be due to strong interband transitions in this range [11]. The high absorbance of the doped Y_2O_3:8 wt.% CeO_2 thin film is noted from the figure. The value of the direct bandgap energy was estimated from Tauc relation [10]:

$$(\alpha h\nu)^n = B(h\nu - E_g) \quad (3)$$

Where: hν is the photon energy in eV, α is the absorption coefficient in cm^{-1}, B is inversely proportional to amorphousity degree related to the material, while the value of n is 2 for direct transitions. The bandgap energy is obtained by extrapolating the linear part of the $(\alpha h\nu)^2$ versus photon energy $(h\nu)$ plots to the axis, $(\alpha h\nu)^2=0$, as shown in Figure 4 and Table 1. From the table, it can be noted that doping with 4 wt.% CeO_2 gave the maximum value of energy gap. The band energy was also observed to decrease with dopant (6, 8 and 10) wt.%CeO_2 ;The increase of the dopant concentration may have increased the induced defect states, resulting in the decrease of the bandgap energy[7].

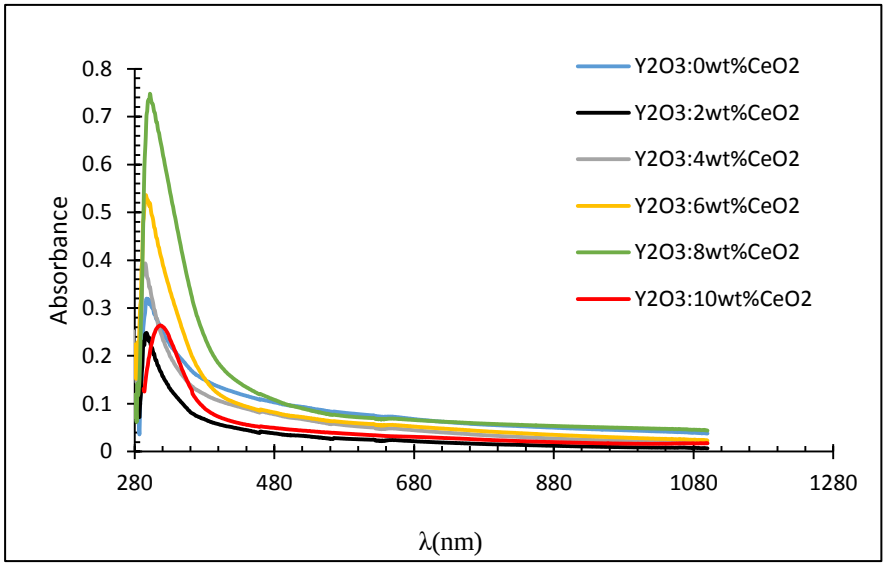

Figure 3- Absorbance spectra for undoped Y_2O_3 film and doped with (2, 4, 6, 8, and 10)%wt. CeO_2.

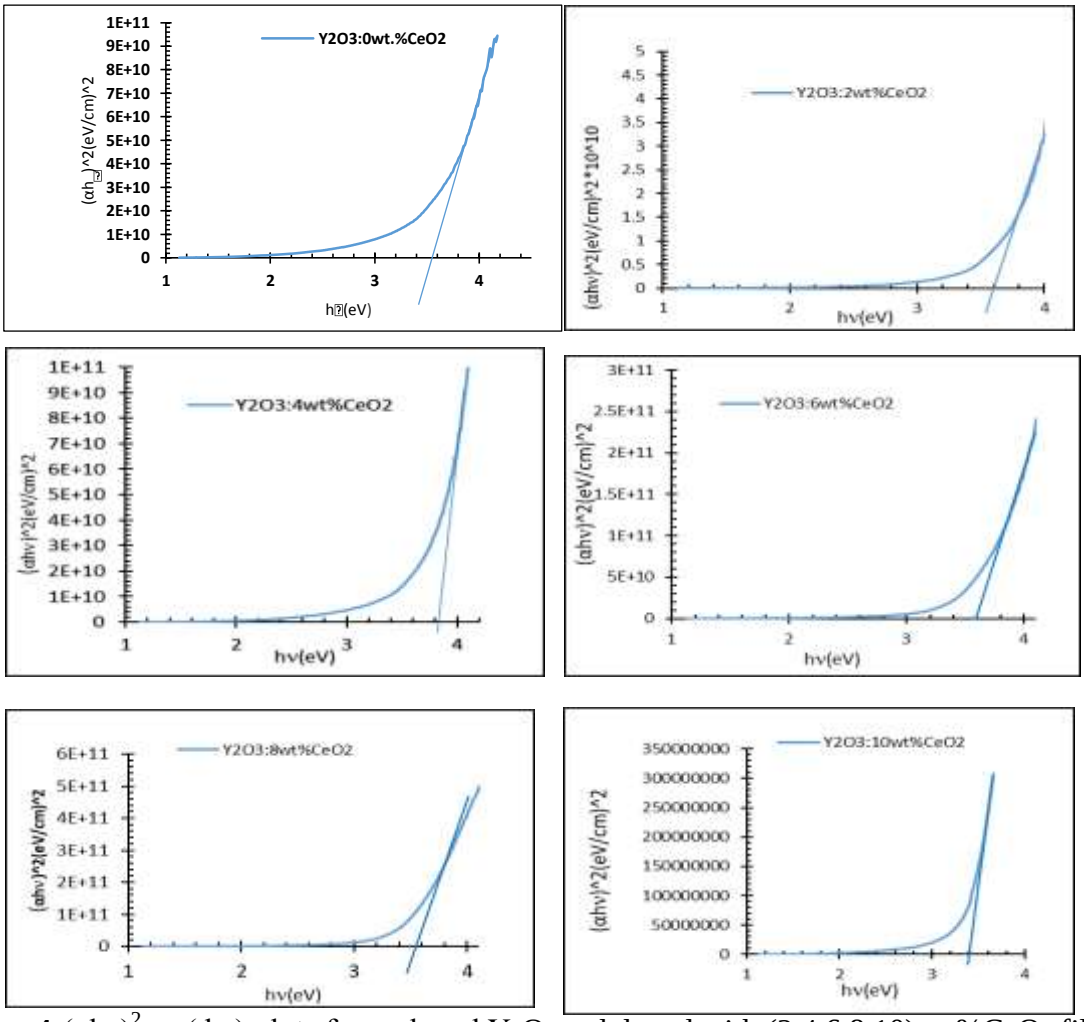

Figure 4-$(\alpha h\nu)^2$ vs.(hν) plots for undoped Y_2O_3 and doped with (2,4,6,8,10)wt.%CeO_2 films

Table 1- Energy gap values, estimated from Tauc relation, of undoped and doped with CeO_2, Y_2O_3 films

CeO_2%	E_g (eV)
0	3.58
2	3.60
4	3.85
6	3.60
8	3.55
10	3.40

2. PL Spectra

The PL spectra of undoped and doped Y_2O_3 thin films are shown in Figure 5. The excitation wavelength (297nm) corresponds to the maximum absorption peak observed in the absorption spectra of the prepared thin films. The emission peak appears at 370 nm at the same wavelength of undoped Y_2O_3 and doped with a slight difference.

By comparing the PL intensity of undoped Y_2O_3 with that of the doped with different ratios of CeO_2, it was observed that Y_2O_3:10wt.%CeO_2 might have higher activity than the other prepared thin films.

The violet light emission peak at 365 nm may be due to the charge transfer from the 4f band to the valence band of Y_2O_3 [12].

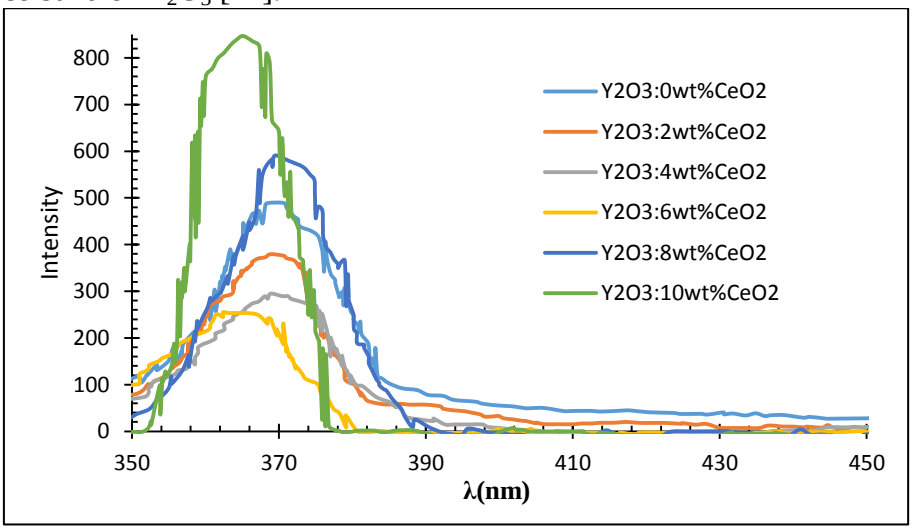

Figure 5- PL spectrum of undoped Y_2O_3 and doped with different ratio of CeO_2

4. Electrical properties

1. Hall Effect measurements

Table 2 shows the Hall coefficient (R_H), the conductivity at room temperature (σ_{RT}), Hall mobility (μ_H), and carriers concentration (n_H) as estimated from the Hall measurements for undoped yttria and doped with (2, 4, 6, 8, and 10) wt.% ceria. Hall measurements showed that all these samples have a positive Hall coefficient (p-type charge carriers) except Y_2O_3:2wt.%CeO_2 which was n-type charge carrier; this means that the doping process affects the type of the charge carriers for Y_2O_2:2Wt.%CeO_2 film. Note that the Hall carrier mobility (μ_H) has fluctuating values ranging between 3.054E+1 cm^2/V.s and- 3.345E+2 cm^2/V.s with the different dopant ratios. The sample Y_2O_3:6wt.%CeO_2 has a high mobility maybe due to its low charge carrier density. The Hall carrier mobility was calculated by the following formula [13]:

$$\mu_H = \frac{\sigma}{n_H.E} \quad (4)$$

Where *q* is electron charge.

Table 2- Hall measurements results for undoped Y_2O_3 and doped with different ratios of (2, 4, 6, 8, and 10) %wt. CeO_2 films.

Sample	σ_{RT} ($ohm^{-1}.cm^{-1}$)	R_H (cm^3/C)	n (cm^{-3})	type	μ_H ($cm^2/V.sec$)
0%	5.433E-5	5.277E+6	1.183E+18	p	2.867E+2
2%	2.770E-5	-8.061E+6	-7.743E+11	n	2.223E+2
4%	2.641E-5	3.872E+6	1.612E+12	p	1.022E+2
6%	3.415E-5	9.795E+6	6.373E+11	p	3.345E+2
8%	2.570E-5	1.189E+6	5.252E+12	p	3.054E+1
10%	2.803E-5	2.120E+6	2.945E+12	p	5.942E+1

2. D.C. Conductivity

The DC electrical conductivity σ as a function of temperature in the temperature range (303-473)^{o}K for undoped and doped Y_2O_3 thin films with different ratios (2, 4, 6, 8, and 10) %wt. of CeO_2 was measured. It can be seen that the electrical conductivity increased with the increase in temperature, displaying a semiconductor like behavior.

The activation energy and conductivity at room temperature of the prepared thin films were determined using Equation (5) [14,15]:

$$\sigma(T) = \sigma_0 \exp\left(-\frac{E_a}{K_B T}\right) \quad (5)$$

where: σ is conductivity at temperature (T), σ_o is a constant, K_B is Boltzmann constant, T is the absolute temperature, and E_a is the activation energy. From the slope of the linear plots of Ln σ versus 1000/T, as shown in Figure 6.

The figure shows that all films have three activation energies except for Y_2O_3:6wt.%CeO_2 which has two activation energies only; this may be due to the change in structure to crystalline. This was confirmed by the XRD examination of Figure 1.

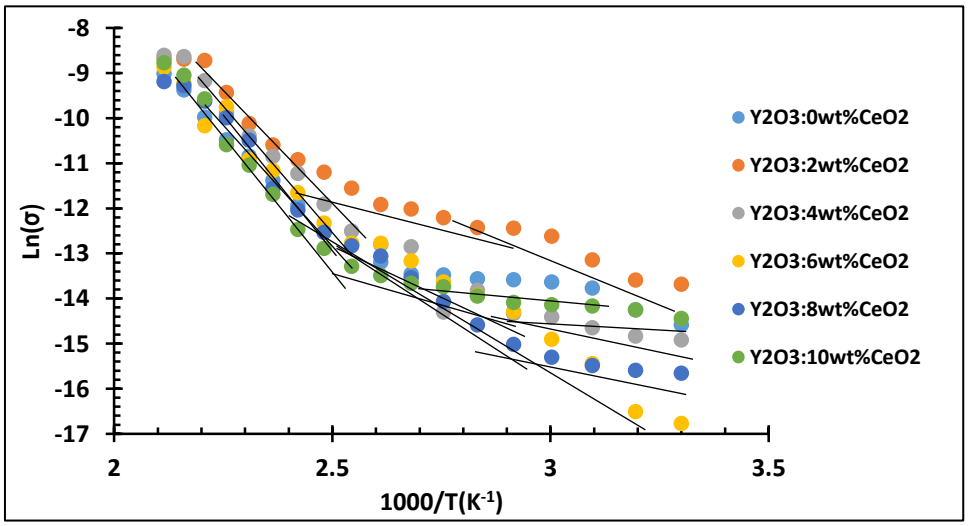

Figure 6-Variation of Ln (σ) with reciprocal temperature for Y_2O_3 doped with CeO_2 at different doping ratios

5. Photoconductive Detector

1. I-V characteristic curves under dark and illumination conditions for Y_2O_3:CeO_2 thin films.

The photoconductivity of the undoped Y_2O_3 films and doped with various weight percentages of CeO_2 (2, 4, 6, 8, and 10) wt % nanostructures deposited on n-Si substrates was determined.

Aluminum (Al) electrodes were attached on top of the prepared films through a metal mask to fabricate a photoconductive detector.

The current-voltage characteristic curves of the films were measured under dark and illumination, at power intensity 288 mW/cm^2, conditions. The dark current and photocurrent against the applied voltage are shown in Figure 7. The increase in photoconductivity is partially due to an increase in the number of the free carriers (electrons and holes), and partially to a decrease in the potential barrier at the grain boundaries, which increases the mobility of the carrier at the grain boundaries, and increases the photoconductivity of the carriers.

It can be noted from this figure that the dark current and photocurrent increased with increasing the voltage bias; at low voltage, the increase of dark current and photocurrent was small because the probability of capturing the free charge carrier by recombination and capture centers, which resulted due to the increase CeO_2, led to the increase of transit time (t_r) between the electrode and thus reducing the mobility and the drift velocity.

Whereas, at high voltage, when the applied electric field on the detector was increased, the drift velocity increased, for this, the defects become unaffected and thus reduced the transit time and the behavior of dark current became linear as a function of high voltage bias. This result is an agreement with Nasir et al. [15]. Schottky behavior of the junction was noticed for the junction of all the fabricated devices except the device Y_2O_3:6wt.%CeO_2 which showed Ohmic behavior because of its crystallinity structure. This was confirmed by the XRD and the DC measurements.

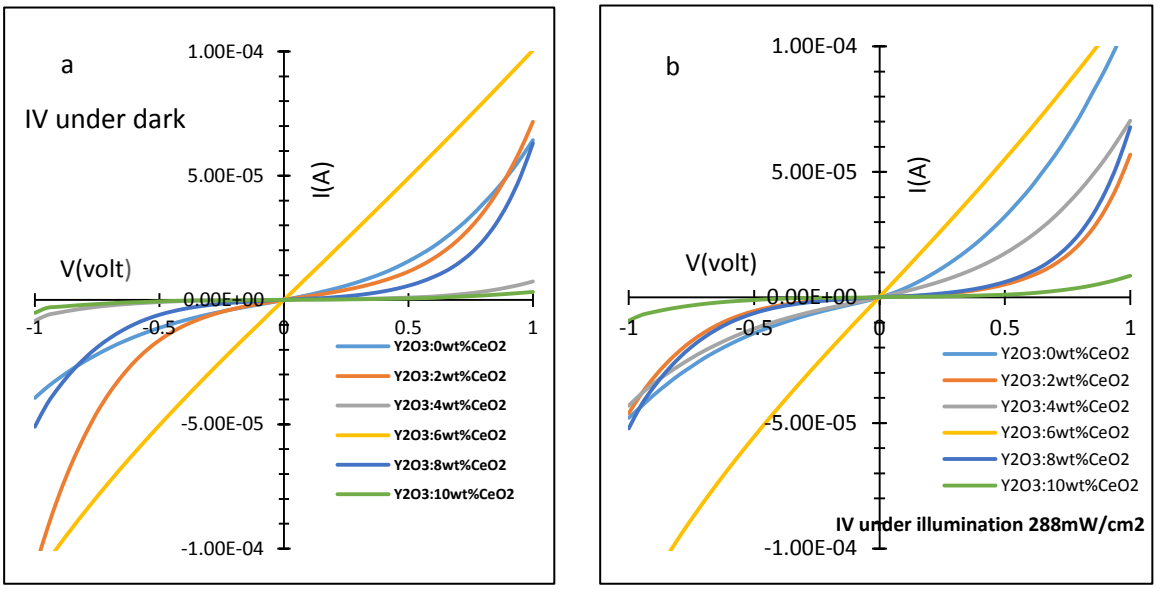

Figure 7- I-V characteristic curves (a) under dark and (b) illumination for undoped Y_2O_3 and doped with different ratios of CeO_2 films.

2. Photosensitivity

Sensitivity (S) is one of the significant parameters that determine the photodetector quality, and is given by [16]:

$$S(\%) = \Delta I_\lambda / I_{dark} \times 100 \quad (6)$$

Where: $\Delta I_\lambda = I_{light} - I_{dark}$ is the photocurrent, I_{light} is the light current, I_{dark} is the dark current.

In simpler terms, sensitivity is a measure of how many current increases in a thin film when subjected to light illumination.

The sensitivity is used to identify the increase in current in a sample under illumination. Conductivity increases when the light is turned on, and after the light is turned off, the current returns to its original value. This process is repeated many times; the rise time and fall time in this process were one second for each state of the (ON, OFF). The current-time (I-t) characteristics are taken with wavelengths of (360,465, 595,659, and 965) nm. The fabricated photoconductive detectorY_2O_3:6wt.%CeO_2 revealed good photosensitivity (high sensitivity) for visible and infrared light. The results are tabulated in Table 3.

Table 3- Variation of sensitivity for undoped Y_2O_3 and doped with different ratio of CeO_2 films.

CeO_2 %	360nm	465nm	595nm	659nm	965nm
0	19.3	1.35	35.15	4.320	17.95
2	19.385	5.053	-	8.633	18.688
4	-	-	4.690	20.126	10.412
6	24.9	120.3	74.071	103.608	107.527
8	-	13.321	-	-	-
10	3.7	-	69.4	46.3	46.7

6. Conclusions

Undoped Y_2O_3 films and doped with CeO_2 nanoparticles were successfully synthesized by the chemical spray pyrolysis method. The XRD measurements confirmed that all the films were amorphous and had three humps. Except Y_2O_3:6wt.%CeO_2 thin film which had signal preferential orientation along the (100) plane belonging to CeO_2. The crystallite size D was 20.3193 nm, $(d_{hkl})_{exp.}$ was found to be equal to 6.943A^o while $(d_{hkl})_{std.}$ was 7.24 A^o
FESEM images illustrated the change of the Y_2O_3:CeO_2 structure from nanorod shape to nanorod and ball shape at higher ceria doping ratio. The absorption spectra of undoped and doped Y_2O_3 films showed the presence of one sharp absorption edge in the UV-Visible region. The optical energy gap of undoped and doped Y_2O_3 had a blue shift with respect. This indicates that quantum confinement happened and the particle size decreased. DC electrical conductivity measurement for the prepared films had three activation energies except for Y_2O_3:6wt.%CeO_2 which had two activation energies. This proves the change in the nature of the synthesized thin films from amorphous to crystalline due to doping at 6wt% CeO_2. Y_2O_3:6wt.%CeO_2 fabricated device showed Ohmic behavior while all the other fabricated devices showed Schottky behavior of the junction. The high sensitivity values of the photo response were obtained from Y_2O_3:6 wt.%CeO_2 for visible and near infrared wavelength.

Acknowledgment

The authors wish to acknowledge the support rendered by the Laboratories of thin films in physical department, College of Science, Baghdad of University.

Reference

[1] S. V. Chavan, P. U. Sastry, A. k. Tyagi," Deagglomeration and fractal behavior of Y2O3 nano-phase powders," *Scripta Mater*, vol. 569, no. 6, p. 569-572, 2006.

[2] Q. Tang, Z. Liu, Sh. Li, Sh. Zang, X. Liu, Y. Qian, "Synthesis of yttrium hydroxide and oxide nanotubes," *Synthes Journal of Crystal Growth*, vol. 259, no. 1-2, pp. 208–214, 2003.

[3] S. Ramanathan, P. Shankar, K. Subramanian, S. S. Ramakrishnan, P. Ch. Angelo, H. Venkataraman "Synthesis of nanocrystalline yttria by sol-gel method," *Materials Letters*, vol. 48, no. 6, p. 342–346, 2001.

[4] Sh. Y. Wang and Z. H. Lu, "Preparation of Y2O3 thin films deposited by pulse ultrasonic spray pyrolysis," *Materials Chemistry and Physics*, vol. 78, no. 2, p. 542–545, 2003.

[5] J. A. Nelson and M. J. Wagner, "Yttrium oxide nanoparticles prepared by alkalide reduction," *Chemistry of Materials*, vol. 14, no. 2, pp. 915–917, 2002.

[6] H. Song, B. Chen, H. Peng, and J. Zhang, "Light-induced change of charge transfer band in nanocrystalline Y2O3:Eu3+," *Applied Physics Letters*, vol. 81, p. 1776–1778, 2002.

[7] G. Bhavani, S. Ganesan, "Structural and Optical study of Yttrium oxide co-doped with bismuth and zinc prepared by sol-gel method," *Indian Journal of pure and Applied Physics*, vol. 54, no. 5, pp. 307-312, 2016.

[8] T. Saravanan, S. G. Raj, N. R. k. Chandar, R. Jayavel, "Synthesis,Optical and Electrochemical Properties of Y2O3 Nanoparticles Prepared by Co-Precipitation Method," *Journal of Nanoscience and Nanotechnology*, vol. 15, no. 6, pp. 4353_4357, 2015.

[9] S. A. Hamdan and I. M. Ali, "Enhancement of Hydrothermally Co3O4 Thin Films as H2S Gas Sensor by Loading Yttrium Element," *Baghdad Science Journal*, vol. 16, no. 1, supplement issue 1, pp. 221-229., 2019.

[10] S. A. Hamdan, I. M. Ali, "Higher Photo Sensitivity Of Co-Y-Oxide Nano Structure Synthesized By Hydrothermal Method," *Digest Journal of Nanomaterials and Biostructures*, vol. 13, no. 3, pp. 669 – 677, 2018.

[11] M. Fanciulli and G. Scarel, Rare Earth Oxide Thin Films, 2010.

[12] Streetman, "*Solid state electronic devices," 2nd Ed. Engle wood Cliffs*, vol. 1, pp. 17-29, 1980.

[13] F. O. a. M. S. Ali G.A.M., "Electrical Properties of Cobalt Oxide/Silica Nanocomposites Obtained by Sol-Gel Technique," *American Journal of Engineering and Applied Sciences*, vol. 9, no. 1, pp. 12-16, 2016.

[14] A. Louardi, A. Rmili, T. Chtouki, B. Elidrissi, H. Erguig, A. El Bachiri, K. Ammous, and H. Mejbri "Effect of annealing treatment on Co3O4 thin films properties prepared by spray pyrolysis," *JMES*, vol. 8, no. 2, pp. 485-493, 2017.

[15] K.M. Chahrour, N.M. Ahmed, M. R. Hashim, N. G. Elfadill, M. Bououdina, "Self-assembly of aligned CuO nanorod arrays using nanoporous anodic alumina template by electro deposition on Si substrate for IR photodetectors," *Sensors and Actuators A: Physical*, vol. 239, pp. 209-219, 2016.

[16] I. M. Ibrahim and A. H. Khalid, "Conjugated Polymer (MEH-PPV: MWCNTs) Organic Nanocomposite for Photodetector Application," *Baghdad Science Journal*, vol. 15, no. 4, pp. 441-448, 2018.

[17] M.F.A. Alias, E. M. N. Al-Fawade, A. A. Alnajjar, A.A.J. Al-douri "Fabrication Of Pbxs1-X Films Photoconductive Detectors," University of Sharjah *Journal of Pure & Applied Sciences*, vol. 3 , no. 3, pp. 1-24, 2006.